

This work was written as part of one of the author's official duties as an Employee of the United States Government and is therefore a work of the United States Government. In accordance with 17 U.S.C. 105, no copyright protection is available for such works under U.S. Law.

Public Domain Mark 1.0

<https://creativecommons.org/publicdomain/mark/1.0/>

Access to this work was provided by the University of Maryland, Baltimore County (UMBC) ScholarWorks@UMBC digital repository on the Maryland Shared Open Access (MD-SOAR) platform.

**Please provide feedback**

Please support the ScholarWorks@UMBC repository by emailing [scholarworks-group@umbc.edu](mailto:scholarworks-group@umbc.edu) and telling us what having access to this work means to you and why it's important to you. Thank you.

RESEARCH ARTICLE | NOVEMBER 30 2011

## Governing factors in stress response of nanoparticle films on water surface

Kyungil Kim; Brian D. Leahy; Yeling Dai; Oleg Shpyrko; Janet S. Soltau; Matthew Pelton; Mati Meron; Binhua Lin



*Journal of Applied Physics* 110, 102218 (2011)

<https://doi.org/10.1063/1.3661988>



Export  
Citation

CrossMark

500 kHz or 8.5 GHz?  
And all the ranges in between.

Lock-in Amplifiers for your periodic signal measurements



Find out more



# Governing factors in stress response of nanoparticle films on water surface

Kyungil Kim,<sup>1</sup> Brian D. Leahy,<sup>1</sup> Yeling Dai,<sup>2</sup> Oleg Shpyrko,<sup>2</sup> Janet S. Soltau,<sup>1</sup> Matthew Pelton,<sup>3</sup> Mati Meron,<sup>1,a)</sup> and Binhua Lin<sup>1</sup>

<sup>1</sup>CARS, University of Chicago, Chicago, Illinois 60637, USA

<sup>2</sup>Department of Physics, University of California-San Diego, San Diego, California 92093, USA

<sup>3</sup>Center for Nanoscale Materials, Argonne National Laboratory, Argonne, Illinois 60439-4806, USA

(Received 16 October 2010; accepted 4 April 2011; published online 30 November 2011)

The mechanical properties of self-assembled silver nanoparticle (Ag-NP) films at the air-liquid interface are studied using both visible light optics and x-ray scattering techniques. The response of such films to compression is compared with results from previously studied gold nanoparticle (Au-NP) films, showing many similarities, along with significant differences. Possible factors governing the stress response of nanoparticle films are discussed. © 2011 American Institute of Physics. [doi:10.1063/1.3661988]

## I. INTRODUCTION

Metal core nanoparticles encapsulated with organic ligands self-assemble into thin films at air-liquid interfaces that exhibit unique mechanical, optical, magnetic, and electrical properties. In recent years, such films have been the topic of many studies due to their potential for various applications, such as MRI treatments, optical applications, catalysts, data storage devices, and magnetic fluids.<sup>1–3</sup>

Under compression, films at air-liquid interfaces exhibit a rich mechanical behavior. Transitions from monolayers to multilayers are observed as are, under some circumstances, various patterns of out-of-plane buckling. These may include the appearance of crisscross hash patterns, ordered periodic wrinkles (perpendicular to the direction of compression) and large scale folds. The specific behaviors observed and their magnitudes may depend upon a variety of factors such as nanoparticle size and polydispersity, the ratio of core to ligand length,<sup>4,5</sup> the composition of the subphase, and the noble metal core. For example, 2 nm diameter gold nanoparticles (Au-NP), ligated with dodecanthiol and spread on the surface of water present with a transition from monolayer to bilayer and no buckling patterns are observed even at high surface pressures, above 30 mN/m.<sup>6,7</sup> On the contrary, with 6 nm diameter Au-NPs, bilayers are not observed and under compression the film changes directly from a mono to a trilayer.<sup>8–10</sup> Once the trilayer state is obtained, further compression results in the appearance (in order) of hash patterns, ordered wrinkles, and large folds.<sup>11</sup>

The magnitude and form of the dependence of the stress response of nanoparticle films on the various factors previously listed is still not fully understood. Additional studies will be needed in order to gain a quantitative understanding of the effects involved. In the current study dodecanthiol-ligated silver nanoparticles (Ag-NPs) with a 6 nm diameter core were investigated, with the results being compared with the results of previous studies, involving Au-NPs of the same nominal diameter. Ag-NPs are well known for their

medical applications. They are widely used for antibacterial applications and have lower cytotoxicity than Ag ions.<sup>12</sup> They are potential candidates for targeted drug delivery.<sup>13–15</sup> They also have significant importance in metal-nanoparticle plasmon research, displaying unrivaled optical properties in the visible/near-IR regime.<sup>16,17</sup> Especially, submicron-sized Ag-NPs show a tunable plasmon response to a Langmuir trough compression which can be a potentially useful optical phenomenon.<sup>18</sup> In addition, comparison studies of the same diameter Ag-NPs and Au-NPs are potentially of value for the development of x-ray liquid surface scattering techniques, since the great difference in x-ray absorption between the two makes it possible to separate the absorption effects from all other effects present in grazing incidence x-ray diffraction (GID) and grazing incidence diffuse x-ray scattering out of the specular plane data.<sup>19,20</sup>

The similarities and the differences of the Ag-NP and Au-NP film's mechanical responses are presented in the following sections. Details of the experimental setups and the measurements performed are described in Sec. II of the paper, followed by a summary of the results in Sec. III and a discussion in Sec. IV.

## II. EXPERIMENTAL DETAILS

Dodecanethiol-ligated Ag-NPs and Au-NPs were purchased from Ocean Nanotech. The average diameters of both the Ag-NPs and the Au-NPs, as determined by x-ray reflectivity data and by UV-Vis spectroscopy, are ~6 nm. However, the transmission electron microscopy (TEM) data provided by Ocean Nanotech (see Fig. 1) show that the polydispersity of the Ag-NPs is significantly higher than that of the Au ones. This introduces a certain ambiguity into the data analysis, which will be discussed later.

The Ag-NPs and Au-NPs were suspended in heptane and the concentration of both of the suspensions is 1.0 mg/mL. Thin films of Ag-NPs and Au-NPs on the surface of water, i.e., Langmuir films of the NPs, were prepared using a Langmuir balance technique<sup>21</sup> and the structure and mechanical responses were studied as a function of stress using three different experimental techniques, namely:

<sup>a)</sup>Author to whom correspondence should be addressed. Electronic mail: meron@cars.uchicago.edu.

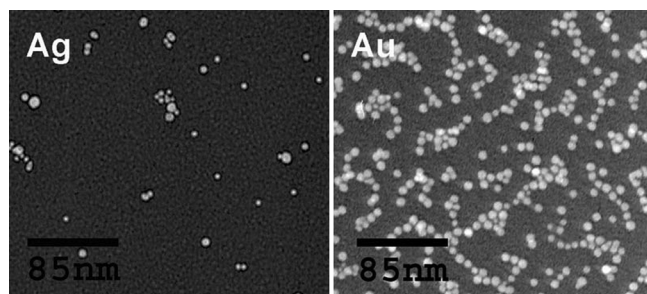


FIG. 1. TEM images of dodecanthiol-ligated silver (left) and gold (right) NPs (provided by Ocean Nanotech). The Ag-NPs are much more polydisperse than the Au-NPs.

- A. Optical microscopy.
- B. UV-Vis absorption spectroscopy.
- C. X-ray liquid surface scattering, including x-ray reflectivity (XR) and grazing incidence x-ray diffraction (GID) measurements.

The first two techniques utilized a NIMA Technology built small microscopy Langmuir trough with two barriers. The x-ray measurements were performed using a custom-built Langmuir trough.

The procedure for the preparation of the Langmuir films of NPs is as follows. The polytetrafluoroethylene trough was cleaned with acetone and chloroform before use. The NP suspensions (concentration of 1mg/mL) were spread on the surface of ultrapure water (Resistivity = 18.2 MΩ) in the trough, using a syringe, and the resulting films were allowed to equilibrate for 15 min before being compressed by the barriers (the speed of compression was 7 mm/min for all of the films). For all of the measurements, the troughs were placed on a vibration isolated table and maintained at room temperature (20–21 °C). During the compression the surface pressure ( $\Pi$ ) and surface area ( $A$ ) were recorded using NIMA software, yielding a  $\Pi$ - $A$  isotherm at the end of the compression, as shown in Fig. 2 (the surface pressure,  $\Pi$ , is defined as the difference between the surface tension of clean water,  $\gamma_0$ , and that of the films at different surface areas,  $\gamma$ ;  $\Pi = \gamma_0 - \gamma$ ). For more details, see Refs. 9, 11, and 22.

### A. Optical microscopy

The morphology of the Langmuir films of the NPs was imaged in a transmission mode using an Olympus optical

microscope equipped with a color CCD camera (Sony 3CCD) and recorded using an HDV mini digital recorder (Sony) as the films were compressed continuously under a constant compression speed of 7 mm/mm. The focusing of the microscope was executed during the image recording using a motorized stage. Typical images, obtained with a total magnification of 125 (a 50× lens and a 2.5× eyepiece) for both of the NP films are shown in Figs. 3 and 4.

### B. UV-Vis measurements

The extinction spectra (the sum of absorption and scattering) of the nanoparticle films were measured in the Center for Nanoscale Materials at Argonne National Laboratory. The measurements were performed using an Olympus IX-71 inverted microscope (10× magnification), with white light (halogen lamp) illumination. The transmitted light was imaged onto the entrance slit of a PI-Acton SpectraPro 2300i spectrometer and dispersed, using a grating, onto an Andor Newton CCD camera. The trough was aligned with the spectrometer slit being perpendicular to the direction of compression. A reference spectrum was recorded before the experiments using the same white-light source, under the same imaging conditions.

A NIMA mini-Langmuir trough designed for an inverted microscope was used. The samples were prepared the same way as previously described. The extinction spectra were recorded at a rate of 0.08 s/scan as the films were compressed continuously with a constant speed of 7 mm/min. Since the barriers moved very slowly, there was very little variation within 20 to 30 consecutive scans. Therefore, groups of 25 scans were combined to produce an average spectrum (see Figs. 5(a) and 5(b)) along the isotherm. The optical scans started at the start of the compression but continued for a few minutes after the compression was completed. The whole compression lasted about 15–20 min.

### C. X-ray measurements

X-ray experiments were conducted with a liquid surface scattering spectrometer<sup>23</sup> at ChemMatCARS, Sector 15 at the Advanced Photon Source, at Argonne National Laboratories. The wavelength of the x-ray beam used was 1.24 Å. The XR measurements were used to probe the film structure in the direction normal to the air-water interface and to provide evidence of layering. The GID measurements provided

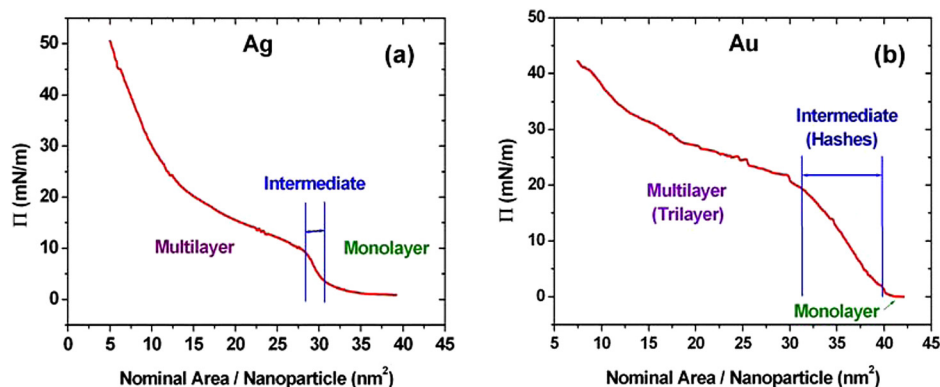


FIG. 2. (Color online) Surface pressure ( $\Pi$ )-surface area isotherms of Langmuir films of (a) Ag-NPs, and (b) Au-NPs. Intervals between the blue-colored lines represent the intermediate (transition) states from monolayer to multilayer.



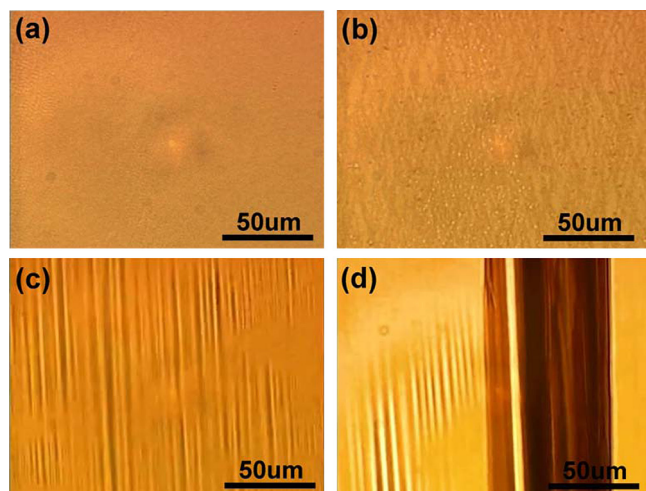


FIG. 3. (Color online) Optical microscope images of morphology transitions of a Ag-NP film under lateral stress, changing from a monolayer (a), to a hash (intermediate) phase (b), to a bilayer (not shown) before wrinkling, with a wrinkle wavelength,  $\lambda = (1.8 \pm 0.2) \mu\text{m}$  (c), and finally to giant folds (d).

information about the in-plane structure of the nanoparticle films, especially information about regular 2-D crystalline ordering. Both XR and GID data were collected with an area detector (Pilatus 100 K).

The custom trough used for the x-ray measurements was enclosed in a hermetically sealed box and equipped with one Teflon block barrier and a Wilhelmy plate tensiometer, both of which are controlled by an interface unit from Nima Technology.<sup>9</sup> The surface density and surface pressure were recorded *in situ* as the x-ray scattering data were collected. The interior of the box was purged and filled with helium, in order to minimize x-ray scattering.<sup>9</sup> The scattering measurements were done at a few fixed surface areas in monolayer and multilayer phases.

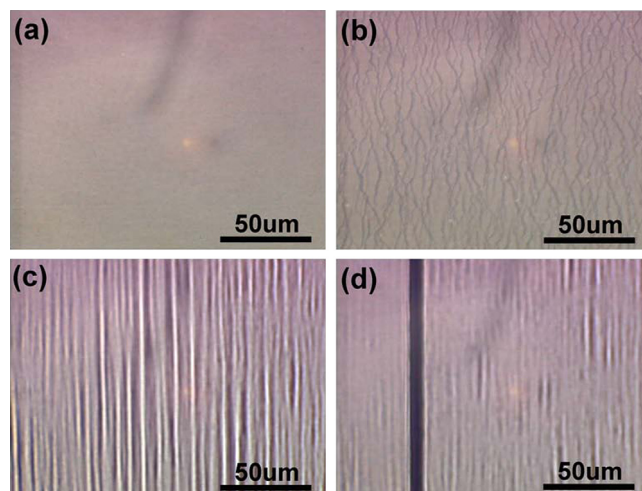


FIG. 4. (Color online) Optical microscope images of morphology transitions of an Au-NP film under lateral stress, changing from a monolayer (a), to a hash (intermediate) phase (b), to a trilayer (not shown) before wrinkling, with a wrinkle wavelength,  $\lambda = (2.7 \pm 0.5) \mu\text{m}$  (c), and finally to giant folds (d).

Two technical problems were encountered in the x-ray measurements; one was that the x-ray surface reflection of the NP films was not homogeneous throughout the trough even though the films appeared optically homogeneous (e.g., Figs. 3(a) and 4(a)), and the other was that the radiation damage of the films was non-negligible. We circumvented the first problem by performing surface reflection scans with beams with a cross section small enough to select surface regions that were homogeneous over the footprints of the x-ray beam. For the second problem, we minimized the radiation damage of the sample by reducing the exposure time and frequently translating the sample relative to the x-ray beam to provide a fresh reflecting surface for consecutive scans.

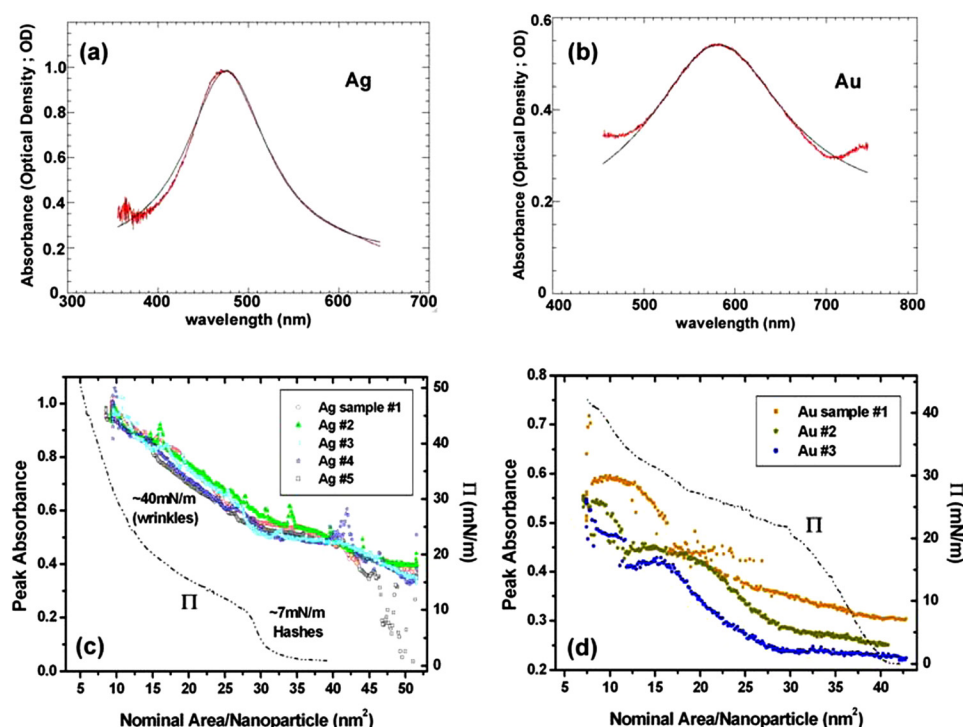


FIG. 5. (Color online) Typical UV-Vis absorption spectra (jagged curves, red online) of an Ag-NP Langmuir film (a) and Au-NP Langmuir film (b), at a fixed area-per-nanoparticle along the isotherm (see Fig. 4), fitted with a Lorentzian function plus a linear background (smooth black curves). The Lorentzian shape is clearly visible. Peak values of the UV-Vis absorption spectra as a function of area-per-nanoparticle for the Ag-NP Langmuir films (c), and the Au-NP Langmuir films (d), juxtaposed with the corresponding isotherms.

### III. RESULTS

#### A. Optical microscopy

The preparation of Ag and Au-nanoparticle films on the surface of water is aided by the coloration of these films (yellow for silver, purple for gold; see Figs. 3 and 4), caused by the surface plasmon resonance. This enables a direct visual observation of the degree of surface coverage, and a microscopic observation of the development of out of plane structures which occurs while the films are being compressed. Based on the visual appearance of these structures, the morphology of the Au-NP and Ag-NP Langmuir films can be divided into three different stages: monolayer, intermediate, and multilayer phases. Transitions between the stages are reflected in the changes of the average isotherm slope and curvature.

Typical Ag-NP and Au-NP isotherms at the air-water interface, recorded at room temperature with the NIMA trough attached to the Olympus optical microscope, are shown in Fig. 2, with the three compression stages being marked. During the monolayer phase of compression, macroscopic film islands are being gathered together like rigid “puzzle pieces.” The islands rotate and break apart to accommodate each other until the visible gaps are reduced. By the end of this phase a visibly uniform monolayer film is observed (Figs. 3(a) and 4(a)).

The intermediate phase, corresponding to monolayer to multilayer transition and hash formation, is much shorter for the Ag-NPs than for the Au-NPs, as shown in the isotherms in Fig. 2, making it more difficult to detect and record the hash patterns. Nevertheless, our observations confirmed that the hash patterns do appear in the Ag-NP film and are similar in appearance to those observed for Au-NPs (Figs. 3(b) and 4(b)). The hash patterns present as jagged and nearly randomly oriented lines which, under further compression, merge and disappear. By the end of this phase, a multilayer (as confirmed by x-ray observations, see the following text) film is obtained.

In the third phase, the continued compression of the multilayers produces periodic wrinkles which appear as dark lines, a few micrometers in wavelength, generally running parallel to the edge of the inward moving barriers (Figs. 3(c) and 4(c)). Under further compression, some of the wrinkles become folds. The folds may be many centimeters long and are easily visible to the naked eye (Figs. 3(d) and 4(d)).

In general, the phases and associated morphological structures observed for the Ag-NP films are similar to those previously observed for the Au-NP films.<sup>11</sup> However, significant differences are also present. As mentioned in the preceding text, the intermediate phase is much shorter for the Ag-NPs than for the 6 nm Au-NPs. In fact, the overall isotherm pattern of the 6 nm (nominal) Ag-NPs resembles that of the 2 nm-core Au-NPs with dodecanthiol ligands.<sup>6</sup> In addition, the Ag-NP wrinkles start to relax when the compression stops and mostly disappear within 3 min, while the wrinkles in the Au-NP films show persistence and relax only under decompression. The Ag-NP folds are scarcer in number than those appearing within the Au-NP films. The wrinkle wavelength of the Ag-NP films is  $1.8 \pm 0.2 \mu\text{m}$ , which is

considerably shorter than the corresponding wavelength for the Au-NPs, which is  $2.7 \pm 0.5 \mu\text{m}$ . Using the relationship,  $\lambda \approx 2\pi(B/\rho g)^{1/4}$  ( $\lambda$ : wrinkle wavelength,  $B$ : the bending rigidity of the film,  $\rho$ : the density of the subphase,  $g$ : the gravitational acceleration),<sup>24–26</sup> the bending rigidity value for the Ag-NP films evaluates to  $\sim 0.02 k_B T$ , which is about 5 times lower than the  $0.1 k_B T$  value obtained for Au-NPs.

#### B. UV-Vis measurements

Although the extinction spectrum includes both absorption and scattering, absorption dominates for the NP sizes used. The interaction of the visible light with the metal cores of the nanoparticles is well described by the classical Mie theory, which predicts an approximately Lorentzian dependence of the absorption profile on the light's frequency.<sup>27</sup> While the amplitude of the absorbance peak is proportional to the optical thickness of the nanoparticle film, changes in the location and width of the peak may provide additional information about possible modifications of the dielectric constant of the nanoparticle's immediate neighborhood.<sup>28–30</sup>

The absorbance of the silver and gold-NP films was measured while the films were being compressed. Typical absorption spectra are shown in Figs. 5(a) and 5(b) for the films of the Ag-NPs and the Au-NPs, respectively. The data were fitted to a sum of a Lorentzian and a linear background in order to obtain peak absorbance values (along with peak locations and widths).

After reaching the fold-formation point, the compression was stopped while the measurement continued for an additional span of time. The measured peak-absorbance curves for a number of different Ag-NP and Au-NP films are shown in Figs. 5(c)–5(d), together with the corresponding isotherms. Since, during compression, surface pressure only begins to notably increase once a complete monolayer has been formed while absorbance is already growing during the “island compression” phase, the pressure and peak-absorbance curves behave differently at this stage. Once a monolayer has been formed, though, surface pressure and peak-absorbance curves display similar trends and exhibit similar slope changes at phase boundaries.

The measured absorbance curves for the five Ag-NP films mostly coalesce into a single curve, within error limits. Since the peak-absorbance values are, in general, proportional to the optical thickness of the film,<sup>31,32</sup> the results indicate that the compressed multilayer thickness is approximately double that of the monolayer, thus the silver multilayer is a bilayer. Once the compression is stopped the film absorbance does not change with time, indicating that the thickness of the film remains steady, even though (as previously mentioned) the wrinkles in the film are being relaxed at this stage.

For reasons not yet quite clear, the variability of the absorbance values for three different Au-NP films is much larger than that for the Ag-NP ones. Therefore, the UV-Vis data from the Au-NP films could not provide a clear answer regarding the thickness of the multilayer (such an answer has been obtained, though, using the x-ray data in the following section). We believe that the enhanced variability of optical absorbance for the Au-NP films is due to the gold films being

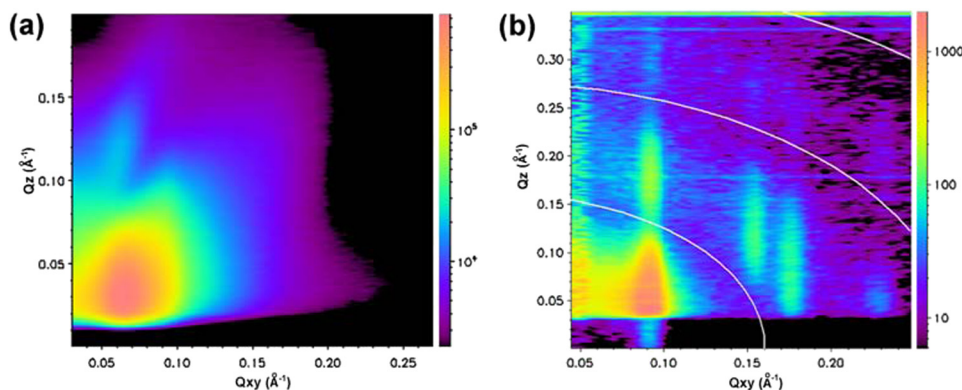


FIG. 6. (Color online) Grazing incidence x-ray diffraction (GID) patterns from monolayers of Ag-NPs (at  $\Pi = 2.7$  mN/m) (a), and Au-NPs (at  $\Pi = 5$  mN/m) (b). The GID data from the monolayer of Ag-NPs do not show any higher order diffraction peaks, while the GID data from the monolayer of the Au-NPs display diffraction peaks up to 4th order. Superimposed white rings on the GID pattern in (b) show the locations of minima of the form factor for a solid sphere 56 Å in diameter.

less homogenous. The presence of even a small fraction of “thinner regions” may notably skew the outcome of an optical transmission measurement, even while the effect on the XR measurement may be unnoticeable.

In principle, the locations of the peak centers and the values of the peak widths in the UV-Vis absorption curves are also of interest, as their variation during compression may provide information about the local strain fields within the films.<sup>30,32</sup> However, these changes within our data were too small to be conclusive.

### C. X-ray measurements

The GID (grazing incidence x-ray diffraction) data provide information about the in-plane arrangement of the scattering particles. Typical GID data for Ag and Au-NP monolayers are shown in Fig. 6. The difference between the two data sets is striking. In the case of the Au-NPs, multiple diffraction rods are present. The spacing of these rods allows for their identification as the 1–4 diffraction orders of a hexagonal 2-D crystalline structure, with an average crystalline domain size (as determined by the width of the peaks) of  $\sim 42$  nm (6–7 particles). In addition, the circular nodes of the single gold nanosphere form factor are present. Their Q-space radius corresponds to an average Au-NP core size of 5.6 nm.

In contrast to the preceding text, only a single peak is present in the GID data from the Ag-NP monolayer. The location of this peak corresponds to a mean nearest neighbor distance of  $9.3 \pm 0.1$  nm, which is larger than the distance of  $7.4 \pm 0.1$  nm measured for the Au-NPs. Neither higher order diffraction peaks nor form factor nodes have been observed in any of the Ag-NP GID data. The absence of form factor nodes is consistent with the polydispersity of the Ag-NPs. The absence of diffraction peaks indicates that the Ag-NP film in-plane structure is that of an amorphous solid, or jammed liquid, unlike the case for the gold film. Again, this is consistent with the polydispersity of the Ag-NPs.

The electron density profile of the films in a direction normal to the water-air interface can be deduced from XR (x-ray reflectivity) measurements. Figure 7 shows the XR data for the Ag-NP films at the monolayer ( $\Pi \sim 2$  mN/m) and the multilayer ( $\Pi \sim 20$  mN/m) phases. The corresponding density profiles were obtained through model independent fitting, using the StochFit software<sup>33</sup> (Fig. 7). The data was also fitted using a 30-layer Parratt’s model, combined with a

capillary wave term.<sup>19</sup> The results were nearly identical. The thickness of the Ag-NP monolayer is about 6 nm, as inferred from the fitting. The multilayer density profile presents with two peaks, indicating a bilayer, consistent with the UV-Vis results. The thickness of the bilayer, as inferred from the fitting, is  $\sim 14$  nm. The fact that it is more than twice the thickness of a monolayer is to be expected, since the Ag-NPs in the bilayer are separated by a layer of ligands.

Comparable results for the gold NP films are shown in Fig. 8. In this case the multilayer density profile, showing three peaks, is a trilayer.

### IV. DISCUSSION

We have investigated the stress response of Ag-NP films at the air-water interface, comparing it with the previously measured stress response of the Au-NP films. The mean size of the noble metal cores, as revealed by our optical and x-ray measurements, was the same for both cases. However, the polydispersity of the Ag-NPs was much larger than that of the Au-NPs.

Under compression, both types of films qualitatively exhibited the same behavior, going through the same three phases: monolayer, hash, and multilayer, with wrinkles (and, eventually, folds) developing in the multilayer phase upon further compression. However, significant differences were also apparent, namely:

1. The Au-NP monolayer film exhibited a clear 2-D hexagonal surface structure, as evidenced by the x-ray GID data. No such structure has been observed in the Ag-NP monolayer films which appear to be amorphous.
2. The surface pressure range corresponding to the hash phase in the Ag-NP film was much shorter than that for the Au-NP film.
3. In the multilayer phase, the Au-NPs form a trilayer structure while a bilayer is observed in the Ag-NPs films.

At present, little is known about the dependence of the mechanical properties of nanoparticle films on the chemical identity of the nanoparticle cores. Since, even at high compression, the metal cores are separated by distances of the order of 1–2 nm, which is large in comparison to the range of chemical and van der Waals interaction potentials, it is plausible that the cores simply act as anchors for the ligands, exerting no further influence on the mechanical properties of the films. Still, the possibility that the ligand density depends



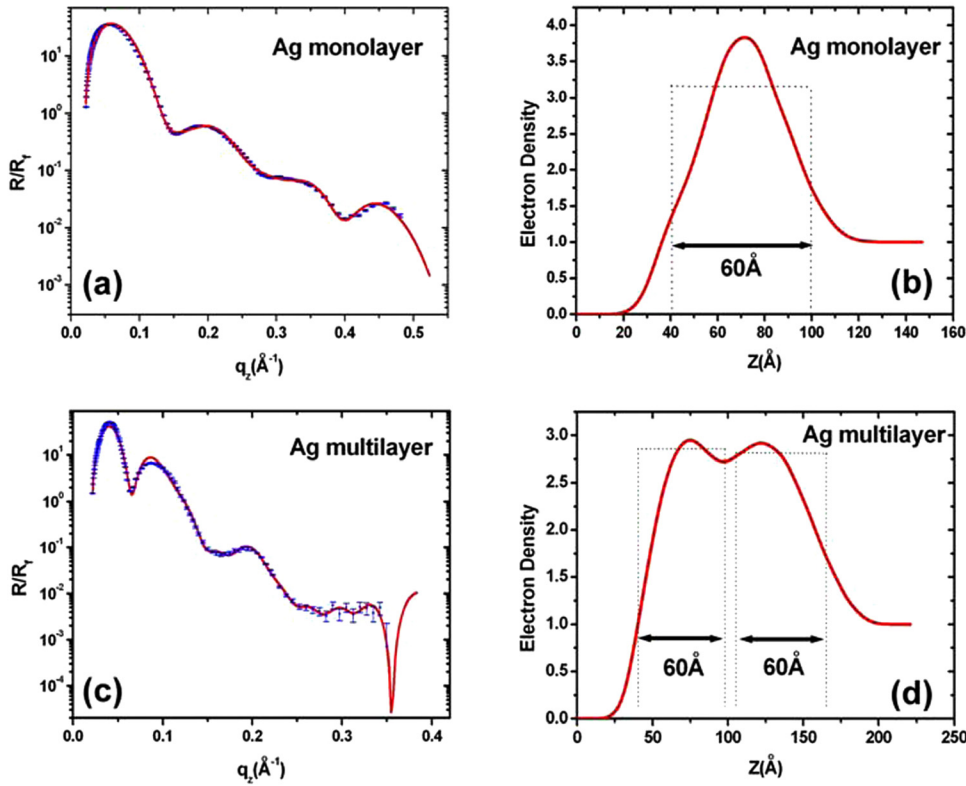


FIG. 7. (Color online) (a) X-ray reflectivity ( $R$ ), normalized by the Fresnel reflection ( $R_F$ ), from the Ag-NP monolayer (symbols) fitted using a model-independent method (StochFit) (solid line). (b) The corresponding electron density profile for the monolayer derived from the fitting. (c) X-ray reflectivity ( $R$ ), normalized by the Fresnel reflection ( $R_F$ ), from the Ag-NP multilayer (symbols) fitted using StochFit (solid line). (d) The corresponding electron density profile for the multilayer. A bilayer structure is clearly visible in the electron density profile in (d). The fitting took into account the Ag-NP's absorption. The dashed line boxes in (b) and (d) illustrate the relationship between the electron density profile and the known nanoparticle diameter.

on the chemical nature of the core cannot be precluded and, if this is the case, one expects the mechanical properties of a nanoparticle film to change when the noble metal core is changed, even if the nanoparticle size remains the same.

At present, we cannot separate the effect of the chemical identity of the NP cores from that of the degree of the poly-

dispersity of the NPs on the mechanical response of the NP films. Nevertheless, our results, together with previous results mentioned here, are consistent with our speculation that the differences listed in the preceding text are mainly due to the difference in polydispersity, not due to the change from gold to silver in the nanoparticle cores. Especially, the

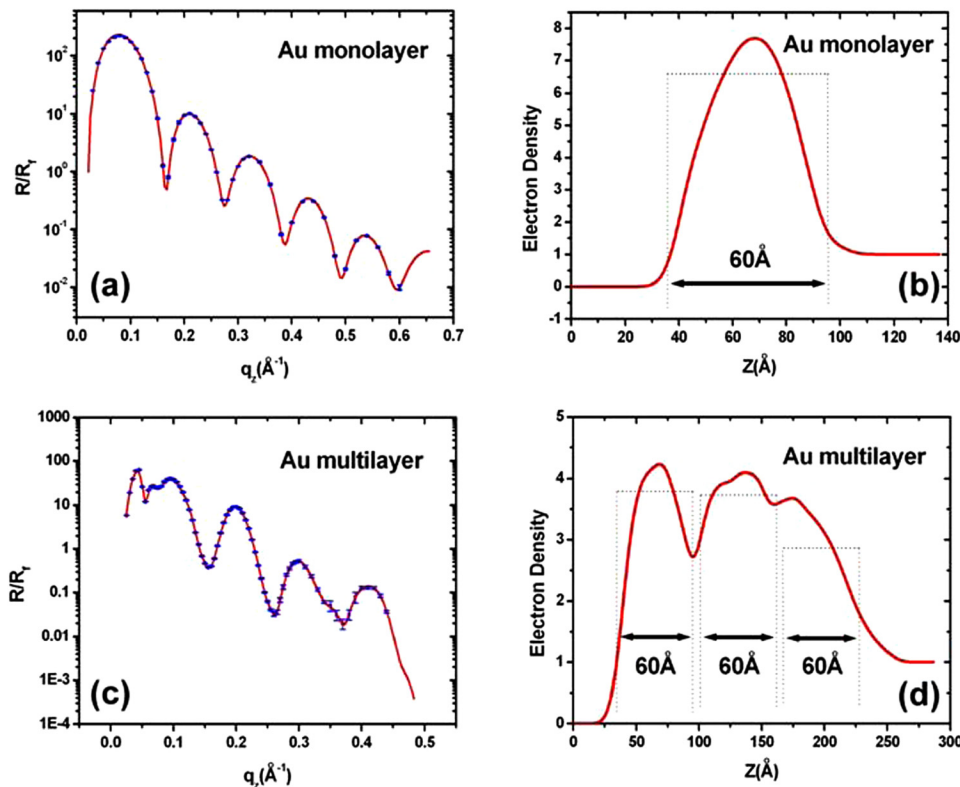


FIG. 8. (Color online) (a) X-ray reflectivity ( $R$ ), normalized by the Fresnel reflection ( $R_F$ ), from Au-NP monolayer (symbols) fitted using a model-independent method (StochFit) (solid line). (b) The corresponding electron density profile for the monolayer derived from the fitting. (c) X-ray reflectivity ( $R$ ), normalized by the Fresnel reflection ( $R_F$ ), from the Au-NP multilayer (symbols) fitted using StochFit (solid line). (d) The corresponding electron density profile for the multilayer, which shows a trilayer structure. The fitting took into account the Au-NP's absorption. The dash line boxes in (b) and (d) illustrate the relationship between the electron density profile and the known nanoparticle diameter.



amorphous structure of the Ag-NP films is most likely due to polydispersity. Since in turn, one expects an amorphous film to be weaker than a corresponding crystalline one, it is plausible that the amorphous films are too fragile to support S-folds, which are the likely explanation for the trilayer formation.<sup>9</sup> However, it is evident that even the low bending rigidity of the bilayers is sufficient to produce stress responses qualitatively similar to those of the gold trilayers.

It may be of interest to study whether the relationship,  $B \sim \text{thickness}^3$ , predicted by macroscopic plate theory, is valid for the thin NP films. However, at present we are unable to vary the film thickness while keeping other parameters (NP size and chemical identity) constant; thus, this question remains open. As mentioned in prior publications<sup>9</sup> it is possible that a monolayer of spherically symmetric nanoparticles exhibits no resistance to bending despite having a finite thickness and Young's modulus. Bending rigidity will still be obtained for the multilayers, due to differential stretching and compressing and a simple-minded model among these lines predict  $B \sim (n-1)^3$ , where  $n$  is the number of layers present. Based on such a model, the bending stiffness of a trilayer should be 4 times larger than that of a monolayer, all else being equal. The ratio of the bending rigidities of the Au-NP trilayer, and the Ag-NP bilayer in our case, based on their corresponding wrinkle wavelengths, is  $\sim 5$  and, since all else is not equal in this case (both the NP chemical identity and their physical separation are different), this result may be consistent with the discrete monolayer model, however, more information is required before any conclusions can be reached.

It is worth mentioning that in prior results by other groups<sup>6,7</sup> different behaviors were observed in the stress responses of Au-NP films, depending on the size of the gold cores. Specifically, no hash patterns, wrinkles, or folds were observed in films produced with 2 nm dodecanthiol-ligated Au-NPs, which is quite unlike the structures observed for the 6 nm Au-NPs. These results were attributed to differences in the core-diameter to ligand-length ratios between smaller and larger NPs. However, since, in general, the polydispersity of NPs increases as the size of the NPs decreases, the different responses observed in those prior measurements could be in part, at least, attributable to differences in the polydispersity, not just to the core-ligand size ratios. With the data available at present, a clear separation of these effects is not possible. It is to be hoped, though, that as the production techniques of nanoparticles keep improving, decoupling of the various effects contributing to the stress response of nanoparticle films will be achieved.

## ACKNOWLEDGMENTS

ChemMatCARS, at the University of Chicago, is supported by the NSF and DOE under Grant No. CHE-0822838. The Advanced Photon Source is supported by the U.S.

Department of Energy, Basic Energy Sciences, Office of Science, under Contract No. W-31-109-Eng-38. Work at UC San Diego is supported by the National Science Foundation CAREER Award Grant 0956131. Use of the Center for Nanoscale Materials was supported by the U.S. Department of Energy, Office of Science, and Office of Basic Energy Sciences, under Contract No. DE-AC02-06CH11357.

- <sup>1</sup>S. Kinge, M. Crego-Calama, and D. N. Reinhoudt, *Chem. Phys. Chem.* **9**(1), 20 (2008).
- <sup>2</sup>W. P. Halperin, *Rev. Mod. Phys.* **58**(3), 533 (1986).
- <sup>3</sup>Z. H. Nie, A. Petukhova, and E. Kumacheva, *Nat. Nanotechnol.* **5**, 15 (2010).
- <sup>4</sup>G. U. Kulkarni, R. J. Thomas, and C. N. R. Rao, *Pure Appl. Chem.* **74**(9), 1581 (2002).
- <sup>5</sup>U. Landman and W. D. Luedtke, *Faraday Discuss.* **125**, 1 (2004).
- <sup>6</sup>M. K. Bera, M. K. Sanyal, S. Pal, J. Dailant, A. Datta, G. U. Kulkarni, D. Luzet, and O. Konovalov, *EPL* **78**(5), 56003 (2007).
- <sup>7</sup>Personal communication and sample sharing for optical microscopy with Sanyal group (Saha Institute of Nuclear Physics, India) (2009).
- <sup>8</sup>D. G. Schultz, X. M. Lin, D. X. Li, J. Gebhardt, M. M. Meron, P. J. Viccaro, and B. Lin, *J. Phys. Chem. B* **110**(48), 24522 (2006).
- <sup>9</sup>B. D. Leahy, L. Pocivavsek, M. M. Meron, K. L. Lam, D. Salas, P. J. Viccaro, K. Y. C. Lee, and B. Lin, *Phys. Rev. Lett.* **105**(5), 058301 (2010).
- <sup>10</sup>L. Pocivavsek, R. Dellsy, A. Kern, S. Johnson, B. Lin, K. Y. C. Lee, and E. Cerda, *Science* **320**(5878), 912 (2008).
- <sup>11</sup>P. W. Li, T. H. Kuo, J. H. Chang, J. M. Yeh, and W. H. Chan, *Toxicol. Lett.* **197**(2), 82 (2010).
- <sup>12</sup>J. W. L. Eccles, U. Bangert, M. Bromfield, P. Christian, and A. J. Harvey, *J. Appl. Phys.* **107**(10), 104325 (2010).
- <sup>13</sup>P. C. Li, D. Li, L. X. Zhang, G. P. Li, and E. K. Wang, *Biomaterials* **29**(26), 3617 (2008).
- <sup>14</sup>P. Ghosh, G. Han, M. De, C. K. Kim, and V. M. Rotello, *Adv. Drug Delivery Rev.* **60**(11), 1307 (2008).
- <sup>15</sup>M. Pelton, J. Aizpurua, and G. Bryant, *Laser Photonics Rev.* **2**(3), 136 (2008).
- <sup>16</sup>A. Tao, P. Sinsermsuksakul, and P. D. Yang, *Angew. Chem., Int. Ed.* **45**(28), 4597 (2006).
- <sup>17</sup>A. Tao, P. Sinsermsuksakul, and P. Yang, *Nat. Nanotechnol.* **2**(7), 435 (2007).
- <sup>18</sup>O. Shpyrko, M. Fukuto, P. Pershan, B. Ocko, I. Kuzmenko, T. Gog, and M. Deutsch, *Phys. Rev. B* **69**(24), 245423 (2004).
- <sup>19</sup>Personal communication with Shpyrko group (Physics, UCSD) (2009).
- <sup>20</sup>V. M. Kaganer, H. Mohwald, and P. Dutta, *Rev. Mod. Phys.* **71**(3), 779 (1999).
- <sup>21</sup>B. Lin, D. G. Schultz, X. M. Lin, D. X. Li, J. Gebhardt, M. M. Meron, and P. J. Viccaro, *Thin Solid Films* **515**(14), 5669 (2007).
- <sup>22</sup>B. Lin, M. M. Meron, J. Gebhardt, T. Graber, M. L. Schlossman, and P. J. Viccaro, *Physica B* **336**(1–2), 75 (2003).
- <sup>23</sup>S. T. Milner, J. F. Joanny, and P. Pincus, *Europhys. Lett.* **9**(5), 495 (1989).
- <sup>24</sup>E. Cerda and L. Mahadevan, *Phys. Rev. Lett.* **90**(7), 074302 (2003).
- <sup>25</sup>Q. Zhang and T. A. Witten, *Phys. Rev. E* **76**(4), 041608 (2007).
- <sup>26</sup>S. Link and M. A. El-Sayed, *J. Phys. Chem. B* **103**(40), 8410 (1999).
- <sup>27</sup>C. Vilain, F. Goettmann, A. Moores, P. Le Floch, and C. Sanchez, *J. Mater. Chem.* **17**(33), 3509 (2007).
- <sup>28</sup>A. Moores and F. Goettmann, *New J. Chem.* **30**(8), 1121 (2006).
- <sup>29</sup>T. Sannomiya, C. Hafner, and J. Voros, *Opt. Lett.* **34**(13), 2009 (2009).
- <sup>30</sup>S. M. Danuskas, D. X. Li, M. M. Meron, B. Lin, and K. Y. C. Lee, *J. Appl. Crystallogr.* **41**, 1187 (2008).
- <sup>31</sup>C. Z. Zhu, S. J. Guo, Y. M. Zhai, and S. J. Dong, *Langmuir* **26**(10), 7614 (2010).
- <sup>32</sup>M. A. Correa-Duarte, V. Salgueirino-Maceira, A. Rinaldi, K. Sieradzki, M. Giersig, and L. M. Liz-Marzan, *Gold Bulletin* **40**(1), 6 (2007).
- <sup>33</sup>S. M. Danuskas, D. X. Li, M. M. Meron, B. Lin, and K. Y. C. Lee, *J. Appl. Crystallogr.* **41**, 1187 (2008).